Buckling of scroll waves

Hans Dierckx,[1] Henri Verschelde,[1] Özgür Selsil,[2] and Vadim N. Biktashev[3]

[1] *Department of Mathematical Physics and Astronomy, Ghent University, Krijgslaan 281, 9000 Ghent, Belgium*

[2] *Department of Mathematical Sciences, University of Liverpool, Liverpool L69 7ZL, UK*

[3] *College of Engineering, Mathematics and Physical Sciences, University of Exeter, Exeter EX4 4QF, UK*

(Dated: September 22, 2012)

A scroll wave in a sufficiently thin layer of an excitable medium with negative filament tension can be stable nevertheless due to filament rigidity. Above a certain critical thickness of the medium, such scroll wave will have a tendency to deform into a buckled, precessing state. Experimentally this will be seen as meandering of the spiral wave on the surface, the amplitude of which grows with the thickness of the layer, until a break-up to scroll wave turbulence happens. We present a simplified theory for this phenomenon and illustrate it with numerical examples.

PACS numbers: 05.45.-a, 87.23.Cc, 82.40.Ck

Spiral waves in two-dimensions, and scroll waves in three-dimensions, are regimes of self-organization observed in physical, chemical and biological dissipative systems, where wave propagation is supported by a source of energy stored in the medium [1, 2]. Due to effective localization of the critical adjoint eigenfunctions, or "response functions" [3, 4], the dynamics of a spiral wave can be asymptotically described as that of pointwise objects, in terms of its instant rotation centre and phase [6]. The third dimension endows scrolls with extra degrees of freedom: the filaments, around which the scroll waves rotate, can bend, and the phase of rotation may vary along the filaments, giving scrolls a twist [7]. The localization of response functions allows description of scroll waves as string-like objects [3, 8–12]. One manifestation of the extra degrees of freedom is the possibility of "scroll wave turbulence" due to negative tension of filaments [13]. It has been speculated that this scroll wave turbulence is in some respects similar to the hydrodynamic turbulence, and may provide insights into the mechanisms of cardiac fibrillation [3, 5, 13, 14].

The motivation for the present study comes from the analogy with hydrodynamics. At intermediate Reynolds numbers, laminar flow can be unstable, leading to non-stationary regimes which are not turbulent [2]. The possibility of similar pre-turbulent regimes in scroll waves is interesting, e.g. in view of its possible relevance to cardiac arrhythmias. Cardiac muscle may be considered quasi-two-dimensional if it is very thin. Since scroll turbulence is essentially three-dimensional, it bears no reflection on behaviour of spiral waves in truly two-dimensional media. Hence the behaviour of scrolls in layers of a given thickness may be effectively two-dimensional, unaffected by the negative tension, or truly three-dimensional, with full blown turbulence, or in an intermediate regime. The understanding of possible intermediate regimes is thus vitally important for interpretation of experimental data and for possible medical implications.

Here we consider one such intermediate regime, which

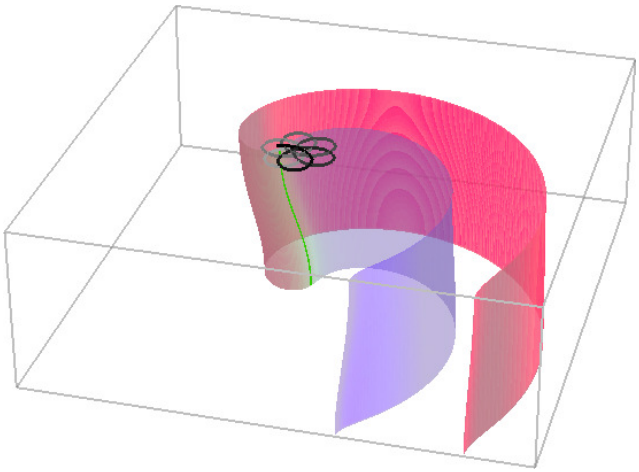

FIG. 1. (color online) Buckled scroll and filament, with the tip path on the top of the box. Barkley model with $a = 1.1$, $b = 0.19$, $c = 0.02$, $D_v = 0.10$, box size $20 \times 20 \times 6.9$ [15].

is illustrated in fig. 1. This is a snapshot of a scroll wave solution of an excitable reaction-diffusion model

$$\partial_t \mathbf{u} = \mathbf{f}(\mathbf{u}) + \mathbf{D}\nabla^2 \mathbf{u}, \tag{1}$$

where $\mathbf{u}, \mathbf{f} \in \mathbb{R}^\ell$, $\mathbf{D} \in \mathbb{R}^{\ell\times\ell}$, $\mathbf{u}(\vec{r}, t)$ is the dynamic vector field, $\vec{r} \in \mathbb{R}^3$, $\mathbf{D}$ is the diffusion matrix and $\mathbf{f}(\mathbf{u})$ are reaction kinetics that sustain rigidly rotating spiral waves, in a rectangular box $\vec{r} = (x, y, z) \in [0, L_x] \times [0, L_y] \times [0, L_z]$, with no-flux boundaries and initial conditions in the form of a slightly perturbed straight scroll. In boxes with L_z below a critical height L_*, the scrolls keep straight and rotate steadily. In large enough L_z, the scroll wave turbulence develops. In a range of L_z slightly above L_* as in fig. 1, the straight scroll is unstable, and its filament, after an initial transient, assumes an S-like shape which remains constant and precesses with a constant angular velocity. In almost any $z =$ const section, including the upper and lower surfaces, one observes spiral waves with a circular core, whose instant rotation centre, in turn,

rotates with an angular speed Ω, which changes little with L_z, but with a radius which is vanishingly small for $L_z \gtrapprox L_*$ and grows with L_z. The resulting tip path, observed on the upper and lower surfaces, is similar to classical two-periodic meander [16]. A similar phenomenon was observed in a model of heart tissue [17].

In this Letter, we investigate the instability which leads to such buckled, precessing filaments, using linear and non-linear theory and numerical simulations. The instability is akin to the Euler's buckling in elasticity, where a straight beam deflects under a compressive stress that is large enough compared to the material's rigidity [18].

Initial insight can be obtained through linearization about a straight scroll wave solution $\mathbf{U}$ stretched along the z-axis, as in [24]. Small perturbations $\tilde{\mathbf{u}}$ with wave number k_z will evolve according to $\partial_t \tilde{\mathbf{u}} = \hat{\mathbf{L}}_{k_z} \tilde{\mathbf{u}}$, where

$$\hat{\mathbf{L}}_{k_z} = \mathbf{D}\nabla^2 - \mathbf{D}k_z^2 + \omega_0 \partial_\theta + \mathbf{f}'(\mathbf{u}_0). \qquad (2)$$

The scroll will be stable if all the eigenvalues to $\hat{\mathbf{L}}_{k_z}$ have negative real part for all allowed wave numbers $k_z = nk_0 = n\pi/L_z$, $n \in \mathbb{Z}$. Analytically, the Taylor expansion in k_z for the critical eigenvalues λ_+, λ_-, associated to translational symmetry,

$$\lambda_\pm(k_z) = \pm i\omega_0 - (\gamma_1 \pm i\gamma_2)k_z^2 - (e_1 \pm ie_2)k_z^4 + \mathcal{O}(k_z^6) \quad (3)$$

relates to overlap integrals of the translational Goldstone modes and response functions [3, 6, 10], see the Appendix [15]. With the notation of [15, 21] and $\hat{\pi} = 1 - |\mathbf{V}_+\rangle \langle \mathbf{W}^+|$, we found

$$\gamma_1 + i\gamma_2 = \langle \mathbf{W}^+ | \, \mathbf{D} \, | \mathbf{V}_+ \rangle \,, \qquad (4)$$

$$e_1 + ie_2 = - \langle \mathbf{W}^+ | \, \mathbf{D} (\hat{\mathbf{L}} - i\omega_0)^{-1} \hat{\pi} \mathbf{D} \, | \mathbf{V}_+ \rangle \,. \qquad (5)$$

Thus, a filament with negative tension γ_1 [3, 10, 11], can nevertheless be stabilized by higher order terms. We call e_1 *filament rigidity*; it is an analogue of the stiffness of an elastic beam, and has the most important stabilizing effect. If $e_1 > 0$, then the leading-order stability condition is

$$k_0 > k_* = \sqrt{-\gamma_1/e_1} \quad \Leftrightarrow \quad L_z < L_* = \pi\sqrt{-e_1/\gamma_1}. \quad (6)$$

When L_z slightly exceeds L_*, a single unstable mode with spatial dependency $\sim \cos \pi z/L_z$ will grow, causing the filament to buckle and precess at a rate

$$\Omega_* = \gamma_1 \left(\gamma_1 e_2 - \gamma_2 e_1\right) / e_1^2. \qquad (7)$$

The amplitude at which the buckling filament will stabilize requires nonlinear analysis. Our full non-linear treatment of this phenomenon based on the time-dependent evolution equation for the scroll filament is rather technical, and we defer it to another publication. Here we will consider simplified scroll dynamics, with the equation of motion of the scroll filament in the form [12]

$$(\dot{\vec{R}})_\perp = \left(\gamma_1 + \gamma_2 \partial_\sigma \vec{R}\times\right) \partial_\sigma^2 \vec{R} - \left(e_1 + e_2 \partial_\sigma \vec{R}\times\right) (\partial_\sigma^4 \vec{R})_\perp + |\partial_\sigma^2 \vec{R}|^2 \left(b_1 + b_2 \partial_\sigma \vec{R}\times\right) \partial_\sigma^2 \vec{R}, \qquad (8)$$

where $\vec{R}(\sigma, t)$ is filament position and σ is arc length. The coefficients b_1, b_2 improve the phenomenological ribbon model proposed in [19]; they relate to the accelerated shrinking of collapsing scroll rings. Linearization of Eq. (8) agrees with Eqs. (6) and (7) above. A filament obeying Eq. (8) at $L_z \approx L_*$ can be represented, in a in a frame precessing with frequency Ω, by its Fourier expansion $[X', Y', Z'] = [A\cos(k_0 z), 0, z] + \ldots$ with $k_0 = \pi/L_z$. Then collecting the terms $\sim \cos k_0 z$ gives

$$\dot{A} = -k_0^2 A \left[(\gamma_1 + e_1 k_0^2) + k_0^2 A^2 q(k_0)\right] = 0, \qquad (9)$$

where $q(k_0) = -\gamma_1/2 + (3b_1/4 - e_1)k_0^2$, which describes a pitchfork bifurcation. By evaluating $q(k_*)$, one finds that the case $b_1 > 2e_1/3$ yields a supercritical bifurcation, with stable branch

$$A_* \approx \frac{L_*}{\pi} \sqrt{\frac{8e_1}{3b_1 - 2e_1}} \sqrt{\frac{L - L_*}{L_*}}, \qquad L_z \to L_*. \qquad (10)$$

In the opposite case, the bifurcation is subcritical.

So, in absence of other instabilities (say two- or three-dimensional meander), and subject to the inequalities $\gamma_1 < 0$, $e_1 > 0$ and the limits of small $|\gamma_1|$ and small $|L_z - L_*|$, we have an approximate solution (6)-(7), (10). The condition of negative tension, $\gamma_1 < 0$, is the key cause of the buckling instability. The condition $e_1 > 0$ ensures that fourth-order arclength derivatives are sufficient to suppress high-wavenumber perturbations and so is important only for particular formulas but not for the phenomenon itself. Violation of the supercriticality condition $b_1 > 2e_1/3$ does not preclude the unstable branch from becoming stable at larger A, as will be seen in fig. 3(c) below. Finally, the conditions $|\gamma_1| \ll 1$, $|L_* - L_z| \ll 1$ are only required for the asymptotics; in reality, one would expect some finite, inter-dependent ranges for γ_1 and L_z to support buckled scrolls. Hence we expect that buckled scrolls are fairly typical and have "finite chances" to be observed in some range of L_z, if only $\gamma_1 < 0$.

In our numerical simulations [15] below, the asymptotics for $\lambda_+(k_z)$ are evaluated using Eqs. (4)-(5), after numerically obtaining the modes $|\mathbf{V}_+\rangle$ and $\langle \mathbf{W}^+|$ using `dxspiral` [20, 21]. These asymptotics are compared to the numerical continuation of $\hat{\mathbf{L}}(k_z)\mathbf{V}(k_z) = \lambda_+(k_z)\mathbf{V}(k_z)$ by the parameter k_z [15].

We used the reaction-diffusion system (1) with Barkley [22] kinetics, $\ell = 2$, $\mathbf{u} = (u, v)$, $\mathbf{f} = (f, g)^{\mathrm{T}}$, $f = c^{-1}u(1-u)(u - (v+b)/a)$, $g = u - v$, and $\mathbf{D} = \mathrm{diag}(1, D_v)$. We mostly use kinetic parameters a, b, c as in [23], which give negative filament tension $\gamma_1 < 0$, and consider also $D_v > 0$ so as to make $|\gamma_1|$ smaller; note that $D_v = 1$ guarantees $\gamma_1 = 1 > 0$.

Fig. 2(a) shows how the buckling amplitude and precession frequency depend on the thickness of the layer, L_z, for the same set of parameters as used to generate fig. 1. We see that just above the bifurcation point,

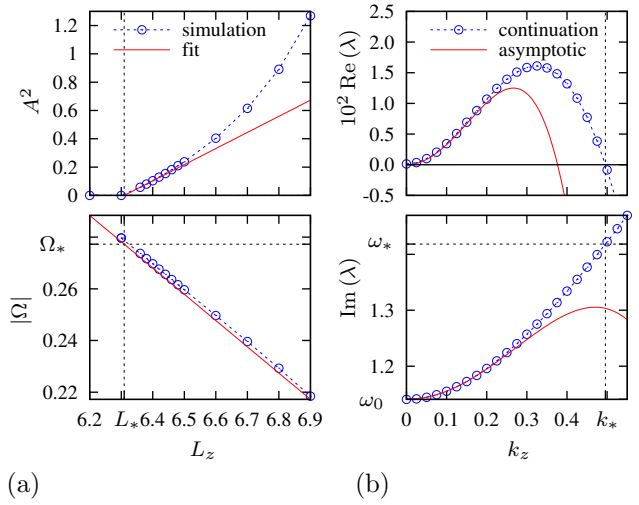

FIG. 2. (color online) (a) Bifurcation diagram ($a = 1.1$, $b = 0.19$, $c = 0.02$, $D_v = 0.1$): the amplitude (upper panel) and precessing frequency (lower panel) of the straight and buckled scrolls. (b) The corresponding translational branch: real part (upper panel) and imaginary part (lower panel). For the meandering mode, $\mathrm{Re}\,(\lambda) < -0.24$ [15].

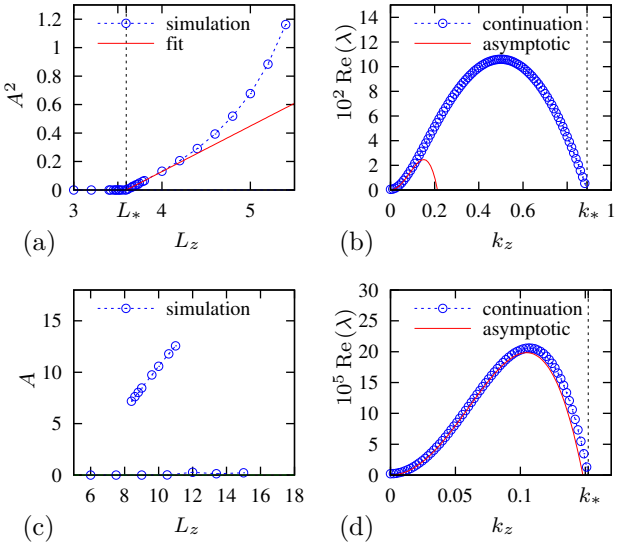

FIG. 3. (color online) (a) Bifurcation diagram (buckling amplitude) and (b) translational branch (real part), for $a = 1.1$, $b = 0.19$, $c = 0.02$, $D_v = 0$. (c,d) Same, for $a = 1.1$, $b = 0.19$, $c = 0.02$, $D_v = 0.25$. For the meandering modes, $\mathrm{Re}\,(\lambda) < -0.098$ and -0.32 respectively [15].

$L_z \gtrapprox L_*$, there is good agreement with Eq. (10). Linear fitting of the $A^2(L_z)$ dependence for the weakest buckled scrolls gives a bifurcation point $L_* \approx 6.310$, and a linear extrapolation of the precessing frequency from the same set gives $\Omega(L_*) \approx 0.2789$. Panel (b) shows the results of the linear analysis, both asymptotic as given by Eq. (3) and obtained by numerical continuation of the eigenvalue problem. The latter gives the $k_* \approx 0.497$, i.e. $L_* = \pi/k_* \approx 6.33$, in agreement with the direct simulations shown in panel (a). The `dxspiral` calculations using Eqs. (4)-(5) give $\gamma_1 = -0.353$, $e_1 \approx 2.49$, resulting in $k_* \approx 0.376$. The nearly 25% difference between the continuation and asymptotic predictions is consistent with k_z being not very small, and should decrease for smaller $|\gamma_1|$. This is indeed true, as seen below. The precessing frequency predicted by continuation is $\Omega_* = \mathrm{Im}\,(\lambda(k_*)) - \omega_0 \approx 1.4188 - 1.1408 = 0.2780$, in agreement with simulations.

Fig. 3 illustrates variations in the buckling bifurcation caused by change of parameter D_v. In panels (a,b), parameters are as in [23] and the filament tension is strongly negative. The `dxspiral` predictions are $\gamma_1 \approx -2.18$, $e_1 \approx 48.2$ so the asymptotic $k_* \approx 0.213$ is vastly different from the continuation prediction $k_* \approx 0.890$, and this discrepancy is clearly visible in panel (b). Yet, panel (a) shows that the bifurcation still takes place, and the critical thickness $L_* \approx 3.60$ is in agreement with the prediction of the continuation, $L_* = \pi/k_* \approx 3.53$. This confirms that the assumption of smallness of the negative tension is only technical and does not preclude buckled scroll solutions, which still occur via a supercritical bifurcation as the medium thickness varies.

Panels (c,d) present a variation where the negative filament tension is much smaller. Panel (d) shows much better agreement between the asymptotics: $\gamma_1 \approx -0.0362$, $e_1 \approx 1.65$, such that $k_* = 0.148$ ($L_* = 21.23$), whereas continuation gives $k_* = 0.152$ ($L_* = 20.66$). However, the bifurcation in this case is subcritical with a hysteresis, see panel (c), which shows that the assumption of supercriticality is not absolute, and that a subcritical bifurcation can likewise lead to buckled scroll solutions.

Finally, we illustrate the difference of the buckling bifurcation we have described here, from the "3D meander" bifurcation described previously [24, 25]. On the formal level, the restabilized scrolls following a 3D meandering instability look similar: at any moment, the filament has a flat sinusoidal shape (given Neumann boundary conditions), and the top and bottom surfaces, as well as almost every $z = \mathrm{const}$ cross-section, show meandering spiral wave pictures. However, the behaviour is completely different as L_z grows, as illustrated in fig. 4. Row (a) shows that in the negative tension case, at sufficiently large L_z the scroll buckles so much it breaks up and a scroll turbulence develops, in agreement with previous results. Row (b) shows that in case of 3D meander, the amplitude remains bounded, and even when L_z is large enough to hold several wavelengths of the curved filament, the restabilized "wrinkled scroll" can persist for a long time (compare these with "zigzag shaped filaments" described in [26]). Moreover, these two bifurcations occur in different parametric regions via different mechanisms. The key diffrence is, apparently, the availability or not of infinitely small unstable wavenumbers [15].

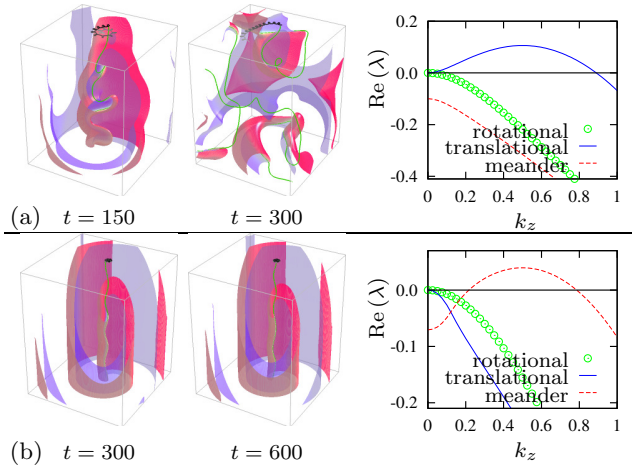

FIG. 4. (color online) Development of (a) autowave turbulence ($a = 1.1$, $b = 0.19$, $c = 0.02$, $D_v = 0$) and (b) "wrinkled scroll" as restabilized solution after 3D meandering bifurcation ($a = 0.66$, $b = 0.01$, $c = 0.025$, $D_v = 0$, which corresponds to the leftmost point of fig.10(a) in [24]).Wavefronts are cut out by clipping planes halfway through the volume, to reveal the filaments. Curves on the right are real parts of rotational, translational and meandering eigenvalue branches of $\hat{\mathbf{L}}_{k_z}$ from Eq. (2).

To summarize, we predict that in an excitable medium with negative nominal filament tension γ_1, a sufficiently thin quasi-two-dimensional layer will nonetheless support transmural filaments which are straight and stabilized by filament rigidity. When the medium thickness L_z is increased beyond a critical thickness L_*, scroll waves may buckle and exhibit an S-shaped, precessing filament. On the surface of the layer this will look like a classical flower-pattern meander. If the system parameters yield a bifurcation of the supercritical type, a stationary buckling amplitude proportional to $\sqrt{L_z - L_*}$ will be reached, at which non-linear filament dynamics compensates for the negative tension γ_1. In the subcritical case, loss of stability of straight scrolls will be abrupt, but it still may lead to restabilized buckled scrolls. The knowledge about the buckling transition and its properties is important for the planning and interpretation of experiments where the medium thickness is comparable to the typical length scale of the spiral wave. In particular, it can be expected that stability of transmural scroll waves in atrial and right ventricular cardiac tissue may in some cases depend on filament rigidity.

Acknowledgments The authors are grateful to I.V. Biktasheva for helpful discussions. The study was supported in part by EPSRC grant EP/D074789/1 and EP/I029664/1 (UK). H.D. acknowledges the FWO-Flanders for personal funding and providing computational infrastructure.

[1] A. M. Zhabotinsky and A. N. Zaikin, in *Oscillatory processes in biological and chemical systems*, edited by E. E. Selkov, A. A. Zhabotinsky, and S. E. Shnol (Nauka, Pushchino, 1971) p. 279; M. A. Allessie, F. I. M. Bonke, and F. J. G. Schopman, Circ. Res. **33**, 54 (1973); F. Alcantara and M. Monk, J. Gen. Microbiol. **85**, 321 (1974); N. A. Gorelova and J. Bures, J. Neurobiol. **14**, 353 (1983); B. F. Madore and W. L. Freedman, Am. Sci. **75**, 252 (1987); S. Jakubith, H. H. Rotermund, W. Engel, A. von Oertzen, and G. Ertl, Phys. Rev. Lett. **65**, 3013 (1990); J. Lechleiter, S. Girard, E. Peralta, and D. Clapham, Science **252** (1991).
[2] M. C. Cross and P. C. Hohenberg, Rev. Mod. Phys. **65**, 851 (1993); T. Frisch, S. Rica, P. Coullet, and J. M. Gilli, Phys. Rev. Lett. **72**, 1471 (1994).
[3] V. N. Biktashev, A. V. Holden, and H. Zhang, Phil. Trans. Roy. Soc. Lond. ser. A **347**, 611 (1994).
[4] I. V. Biktasheva, Y. E. Elkin, and V. N. Biktashev, Phys. Rev. E **57**, 2656 (1998).
[5] R. M. Zaritski, S. F. Mironov, and A. M. Pertsov, Phys. Rev. Lett. **92**, 168302 (2004).
[6] V. Biktashev and A. Holden, Chaos Solitons & Fractals **5**, 575 (1995).
[7] A. T. Winfree and S. H. Strogatz, Physica D **8**, 35 (1983), 9:65–80.
[8] L. Yakushevich, Studia Biophysica **100**, 195 (1984).
[9] P. K. Brazhnik, V. A. Davydov, V. S. Zykov, and A. S. Mikhailov, Zh. Eksp. Teor. Fiz. **93**, 1725 (1987).
[10] J. Keener, Physica D **31**, 269 (1988).
[11] H. Verschelde, H. Dierckx, and O. Bernus, Phys. Rev. Lett. **99**, 168104 (2007).
[12] H. Dierckx, Ph.D. thesis, Ghent University (2010).
[13] V. N. Biktashev, Int. J. of Bifurcation and Chaos **8**, 677 (1998).
[14] A. T. Winfree, Science **266**, 1003 (1994).
[15] See EPAPS Document No. [number will be inserted by publisher] for the Appendix with details of asymptotic and numerical procedures and extra results, and a movie. For more information on EPAPS, see `http://www.aip.org/pubservs/epaps.html`.
[16] V. S. Zykov, Biophysics **31**, 940 (1986).
[17] S. Alonso and A. V. Panfilov, Chaos **17**, 015102 (2007).
[18] L. D. Landau and E. M. Livshitz, *Theory of Elasticity* (Pergamon, Oxford, 1975).
[19] B. Echebarria, V. Hakim, and H. Henry, Phys. Rev. Lett. **96**, 098301 (2006).
[20] D. Barkley, V. N. Biktashev, I. V. Biktasheva, G. V. Bordyugov, and A. J. Foulkes, "DXSpiral: a code for studying spiral waves on a disk," `http://www.csc.liv.ac.uk/~ivb/software/DXSpiral.html`.
[21] I. V. Biktasheva, D. Barkley, V. N. Biktashev, G. V. Bordyugov, and A. J. Foulkes, Phys. Rev. E **79**, 056702 (2009).
[22] D. Barkley, Physica D **49**, 61 (1991).
[23] S. Alonso, R. Kahler, A. S. Mikhailov, and F. Sagues, Phys. Rev. E **70**, 056201 (2004).
[24] H. Henry and V. Hakim, Phys. Rev. E **65**, 046235 (2002).
[25] I. Aranson and I. Mitkov, Phys. Rev. E **58**, 4556 (1998).
[26] C. Luengviriya, U. Storb, G. Lindner, S. C. Müller, M. Bär, and M. J. B. Hauser, Phys. Rev. Lett. **100**, 148302 (2008).

Appendices to "Buckling of scroll waves "
by H. Dierckx, H. Verschelde, Ö. Selsil and V.N. Biktashev

The first appendix is of theoretical nature; it clarifies bracket notation and offers a proof for the rigidity coefficient expression (5). The second appendix provides details on the numerics and processing of simulation data. The third appendix describes extra results that might be of interest for some readers. Enumeration of equations and figures here is continued from that of the main paper, but the list of references is separate.

A. Supplementary material on theory

A.1 Bracket notation for Goldstone modes and response functions

We find it convenient to adopt Dirac's bra-ket notation from quantum mechanics and adapt them to the non-selfadjoint problems we deal with here. Let $\mathcal{V}$ be a suitably chosen linear space of complex-valued m-component vector functions $\mathbf{v} : \mathbb{R}^2 \to \mathbb{C}^m$, the real part of which contains solutions to our reaction-diffusion system. We also consider its dual space, $\mathcal{W} = \mathcal{V}^*$, which corresponds to the space of complex-valued linear functionals $W[\cdot]$ acting on $\mathbf{v} \in \mathcal{V}$. The dual space $\mathcal{W}$ consists of generalized functions $\mathbf{w} : \mathbb{R}^2 \to \mathbb{C}^m$, which define those functionals via

$$W[\mathbf{v}] = \iint\limits_{\mathbb{R}^2} \mathbf{w}^H(x,y)\mathbf{v}(x,y)\,\mathrm{d}x\,\mathrm{d}y = \langle \mathbf{w}|\mathbf{v}\rangle\,. \qquad (11)$$

So we write functions from $\mathcal{V}$ as ket-vectors, and functions from $\mathcal{W}$ as bra-vectors, assuming the scalar product between them when bra-vector is followed by a ket-vector.

An operator $\hat{\mathbf{A}}$ acting in $\mathcal{V}$ has its adjoint operator $\hat{\mathbf{A}}^\dagger$ acting in $\mathcal{W}$, so that for all $\mathbf{v} \in \mathcal{V}$ and $\mathbf{w} \in \mathcal{W}$,

$$\langle \hat{\mathbf{A}}^\dagger \mathbf{w}|\mathbf{v}\rangle = \langle \mathbf{w}|\hat{\mathbf{A}}\mathbf{v}\rangle\,,$$

which is then briefly written as $\langle \mathbf{w}|\,\hat{\mathbf{A}}\,|\mathbf{v}\rangle$.

In the context of spiral waves, one often linearizes the reaction-diffusion system (1)

$$\frac{\partial \mathbf{u}}{\partial t} = \mathbf{f}(\mathbf{u}) + \mathbf{D}\nabla^2\mathbf{u}, \qquad (12)$$

around a rigidly rotating spiral wave solution $\mathbf{U}$, in the frame that rotates with the spiral, to find

$$\hat{\mathbf{L}} = \mathbf{D}\nabla^2 + \omega_0\partial_\theta + \mathbf{f}'(\mathbf{U}),$$
$$\hat{\mathbf{L}}^\dagger = \mathbf{D}^{\mathrm{T}}\nabla^2 - \omega_0\partial_\theta + \mathbf{f}'(\mathbf{U})^{\mathrm{T}},$$

where ω_0 is spiral rotation rate and θ is the polar angle. The Euclidean symmetry of the reaction-diffusion system (12) endows $\hat{\mathbf{L}}$ with three critical eigenvalues

$$\hat{\mathbf{L}}\mathbf{V}_{(n)} = \lambda_{(n)}\mathbf{V}_{(n)},\ \lambda_{(n)} = in\omega_0,\ n \in \{-1,0,1\}.$$

The critical eigenvectors $\mathbf{V}_{(1)}$, $\mathbf{V}_{(-1)}$ which are written $|\mathbf{V}_+\rangle$, $|\mathbf{V}_-\rangle$ here, are sometimes called the translational Goldstone modes; they can be taken in the form

$$|\mathbf{V}_\pm\rangle = -\frac{1}{2}\,|\partial_x\mathbf{U} \pm i\partial_y\mathbf{U}\rangle\,.$$

The spectrum of $\hat{\mathbf{L}}^\dagger$ is the complex conjugate to the spectrum of $\hat{\mathbf{L}}$, and in particular

$$\langle \hat{\mathbf{L}}^\dagger\mathbf{W}^{(n)}| = \langle \bar{\lambda}_{(n)}\mathbf{W}^{(n)}|\,, \quad \lambda_{(n)} = in\omega_0 \qquad (13)$$

(this is actually a nontrivial mathematical fact, see e.g. the discussion in [9]). A common choice of normalization is such that

$$\langle \mathbf{W}^{(m)}|\mathbf{V}_{(n)}\rangle = \delta^m_n, \qquad m,n \in \{-1,0,1\}. \qquad (14)$$

The modes $\langle \mathbf{W}^+|$, $\langle \mathbf{W}^-|$ are known as 'response functions for translation'. Their belonging to $\mathcal{W}$ implies that they are effectively localized in space so that integrals like (11) always converge even though typical functions $\mathbf{v}$ are only bounded but not localized. Again, see [9] for a more detailed discussion.

A.2 Linearized theory

Here we prove the result (5), which expresses the filament rigidity coefficients e_1, e_2 in terms of response functions. We shall make use of a non-selfadjoint version of the Feynman-Hellman theorem, which states how the eigenvalue corresponding to a normalized eigenstate of a self-adjoint operator changes upon the variation of a real-valued parameter. For a non-selfadjoint operator $\hat{\mathbf{A}}$, if $\hat{\mathbf{A}}\,|\mathbf{V}\rangle = \lambda\,|\mathbf{V}\rangle$, $\langle \hat{\mathbf{A}}^\dagger\mathbf{W}| = \langle \bar{\lambda}\mathbf{W}|$ and $\langle \mathbf{W}|\mathbf{V}\rangle = 1$ for all T from a continuous interval, it follows that

$$\langle \partial_T\mathbf{W}|\mathbf{V}\rangle + \langle \mathbf{W}|\partial_T\mathbf{V}\rangle = 0 \qquad (15)$$

and $\lambda = \langle \mathbf{W}|\hat{\mathbf{A}}\mathbf{V}\rangle = \langle \hat{\mathbf{A}}^\dagger\mathbf{W}|\mathbf{V}\rangle$, so

$$\begin{aligned}\partial_T\lambda &= \partial_T\,\langle \mathbf{W}|\,\hat{\mathbf{A}}\,|\mathbf{V}\rangle \\ &= \langle \partial_T\mathbf{W}|\,\hat{\mathbf{A}}\,|\mathbf{V}\rangle + \langle \mathbf{W}|\,\partial_T\hat{\mathbf{A}}\,|\mathbf{V}\rangle + \langle \mathbf{W}|\,\hat{\mathbf{A}}\,|\partial_T\mathbf{V}\rangle \\ &= \langle \mathbf{W}|\,\partial_T\hat{\mathbf{A}}\,|\mathbf{V}\rangle\,. \end{aligned} \qquad (16)$$

We apply this theorem to the operator defined in Eq. (2), i.e. $\hat{\mathbf{A}} = \hat{\mathbf{L}}_{k_z} = \hat{\mathbf{L}} - k_z^2\mathbf{D}$, and parametrize is by $T = k_z^2$. We know about the continuos branches of $|\mathbf{V}(T)\rangle$ and $\langle \mathbf{W}(T)|$, that at $k_z = 0$ they reduce to the translational modes, $|\mathbf{V}(0)\rangle = |\mathbf{V}_+\rangle$ and $\langle \mathbf{W}(0)| = \langle \mathbf{W}_+|$.

Close to $k_z = 0$, we expand

$$\lambda_+ = i\omega_0 - \gamma k_z^2 - e k_z^4 + \mathcal{O}(k_z^6),$$

with yet unknown complex coefficients $\gamma = \gamma_1 + i\gamma_2$, $e = e_1 + ie_2$ (see Eq. (3)). In terms of the parameter $k_z^2 = T$, we will be looking for $\gamma = -\partial_T \lambda_+$ and $e = -\frac{1}{2}\partial_T^2 \lambda_+$, evaluated at $T = 0$. From the Feynman-Hellman theorem (16) it follows

$$\partial_T \lambda_+ = \langle \mathbf{W}| \, \partial_T \hat{\mathbf{L}}_{k_z} \, |\mathbf{V}\rangle = - \langle \mathbf{W}| \, \mathbf{D} \, |\mathbf{V}\rangle \, . \tag{17}$$

Evaluated at $k_z^2 = T = 0$, this recovers the well-known expression for the filament tension coefficient, i.e. $\gamma = \gamma_1 + i\gamma_2 = \langle \mathbf{W}^+| \, \mathbf{D} \, |\mathbf{V}_+\rangle$ [5–7]. Differentiation of Eq. (17) gives

$$-\partial_T^2 \lambda_+(0) = \langle \partial_T \mathbf{W}^+| \, \mathbf{D} \, |\mathbf{V}_+\rangle + \langle \mathbf{W}^+| \, \mathbf{D} \, |\partial_T \mathbf{V}_+\rangle \tag{18}$$

The derivatives of the eigenfunctions can be evaluated by differentiating $\hat{\mathbf{L}}_{k_z} |\mathbf{V}\rangle = \lambda |\mathbf{V}\rangle$ with respect to T, delivering

$$(\hat{\mathbf{L}}_{k_z} - \lambda_+) \, |\partial_T \mathbf{V}\rangle = (\mathbf{D} - \partial_T \lambda_+) \, |\mathbf{V}\rangle \, ,$$

and similarly for $\langle \partial_T \mathbf{W}|$. At $T = 0$, we have $\lambda_+ = \omega_0$, $\partial_T \lambda_+ = \gamma$. We note that the linear equations for $|\partial_T \mathbf{V}\rangle$ and $\langle \partial_T \mathbf{W}|$ are solvable, because their right-hand sides do not have components along the null-space of the linear operator. Namely, it is easy to see that $(\mathbf{D} - \gamma) \, |\mathbf{V}_+\rangle = \hat{\pi} \mathbf{D} \, |\mathbf{V}_+\rangle$ and $\langle \mathbf{W}^+| \, (\mathbf{D} - \gamma) = \langle \mathbf{W}^+| \, \mathbf{D} \hat{\pi}$, where

$$\hat{\pi} = \left(1 - |\mathbf{V}_+\rangle \, \langle \mathbf{W}^+|\right) \tag{19}$$

is the projection operator which kills the components of a vector along the null space of $\hat{\mathbf{L}} - i\omega_0$. With this in mind, we get

$$|\partial_T \mathbf{V}_+\rangle = (\hat{\mathbf{L}} - i\omega_0)^{-1} \hat{\pi} \mathbf{D} \, |\mathbf{V}_+\rangle + C_1 \, |\mathbf{V}_+\rangle \tag{20}$$

$$\langle \partial_T \mathbf{W}^+| = \langle \mathbf{W}_+| \, \mathbf{D} \hat{\pi} (\hat{\mathbf{L}} - i\omega_0)^{-1} + C_2 \, \langle \mathbf{W}^+| \tag{21}$$

where C_1 and C_2 are arbitrary constants, which depend on the choices of normalizations of $|\mathbf{V}\rangle$ and $\langle \mathbf{W}|$ at different values of T. These choices are constrained by Eq. (15), which implies

$$\begin{aligned} 0 = (C_1 + C_2) \, \langle \mathbf{W}^+ | \mathbf{V}_+ \rangle \\ + \langle \mathbf{W}^+| \, \mathbf{D} (\hat{\mathbf{L}} - i\omega_0)^{-1} \hat{\pi} \, |\mathbf{V}_+\rangle \\ + \langle \mathbf{W}^+| \, \hat{\pi} (\hat{\mathbf{L}} - i\omega_0)^{-1} \mathbf{D} \, |\mathbf{V}_+\rangle \\ = C_1 + C_2, \end{aligned} \tag{22}$$

because of the normalization $\langle \mathbf{W}^+ | \mathbf{V}_+ \rangle = 1$ and because $\hat{\pi} \, |\mathbf{V}_+\rangle = |\mathbf{0}\rangle$ and $\langle \mathbf{W}^+| \, \hat{\pi} = \langle \mathbf{0}|$ by definition of $\hat{\pi}$.

Substitution of Eqs. (20) and (21) into Eq. (18), with account of Eq. (22), then delivers

$$\begin{aligned} e_1 + ie_2 = -\frac{1}{2} \partial_T^2 \lambda_+(0) \\ = \langle \mathbf{W}^+| \, \mathbf{D} (\hat{\mathbf{L}} - i\omega_0)^{-1} \hat{\pi} \mathbf{D} \, |\mathbf{V}_+\rangle \, , \end{aligned}$$

which concludes our proof of Eq. (5). Note that both rigidity coefficients vanish for a system with equal diffusion of variables ($\mathbf{D} = D_0 \mathbf{1}$), since $\hat{\pi} \, |\mathbf{V}_+\rangle = |\mathbf{0}\rangle$.

B. Supplementary material on numerical simulations and data processing

B.1 Direct numerical simulations

We used two schemes for forward evolution of the reaction-diffusion system, an explicit and a semi-implicit.

Explicit scheme: Forward Euler in time with step Δ_t, and 7- or 19-point appoximation of the Laplacian with step Δ_x in cuboid domains of size $L_x \times L_y \times L_z$. We used sequential solver EZSCROLL by Barkley and Doyle [1], and our own sequential and MPI-parallel solvers.

Semi-implicit: Operator splitting between reaction and diffusion substeps, with the diffusion substep by Brian's three-dimensional alternating-direction procedure [2, 3] which is unconditionally stable and second-order time accurate, implemented in our own sequential solver.

The initial conditions were in the form of a straight scroll wave with the filament along the z coordinate, slightly perturbed: slightly twisted (z-dependent rotation) or slightly bended (z-dependent shift).

The details specific for different simulation series are listed in Table I. The bifurcation plots in figures 2(a) and 3(a) each were obtained through two series of simulations: one with fixed Δ_x and varied $N_z = L_z/\Delta_x$, and the other, to achieve a finer tuning of L_z, with fixed N_z and varying Δ_x.

TABLE I. Discretization parameters for direct numerical simulations. SI: semi-implicit; E7: explicit with 7-point Laplacian; E19: explicit with 19-point Laplacian.

Figure	Scheme	Δ_t	Δ_x	$L_x = L_y$	L_z
1	SI	1/60	1/10	20	6.9
2(a)	E7	$\Delta_x^2/12$	1/10	16	varied
2(a)	E7	$\Delta_x^2/12$	$L_z/64$	$160\Delta_x$	varied
3(a)	E19	$3\Delta_x^2/16$	1/5	17	varied
3(a)	E19	$3\Delta_x^2/16$	$L_z/19$	$85\Delta_x$	varied
3(c)	E7	$3\Delta_x^2/20$	1/5	120	varied
4(a,b)	E7	$\Delta_x^2/12$	1/5	40	50

B.2 Postprocessing of simulation data

The results of simulations were visualized using a slightly modified graphical part of EZSCROLL, based on the Marching Cubes algorithm [1]. Figures 1 and 4 show snapshots of surfaces $u(x, y, z, t) = u_*$ at selected moments of time, semi-transparent and coloured depending on corresponding values of $v(x, y, z, t)$: red for smaller v, blue for larger v, with a smooth transition at around $v = v_*$. The tip line, which approximates the instanta-

neous filament, was defined as the intersection of isosurfaces $u(x,y,z,y) = u_*$ and $v(x,y,z,t) = v_*$, and is shown in green. The path of the end of the tip line at the upper surface, i.e. the curve defined by $u(x,y,L_z,t) = u_*$ and $v(x,y,L_z,t) = v_*$, is drawn in grayscale, with darker shade corresponding to more recent position. We made the traditional choice for Barkley kinetics, $u_* = 1/2$ and $v_* = a/2 - b$.

The buckling amplitude and precession were defined in two steps. Firstly, at a sufficiently frequent time sampling (t_n), say at least 30 per period, we recorded the positions of the tip line as $X_{m,n} = x(z_m, t_n)$, $Y_{m,n} = y(z_m, t_n)$, with $z_m = m\Delta_x$, $m = 0, \ldots, N_z$, and at each t_n, approximated the tip line by

$$\begin{aligned} X_{m,n} &\approx A_x(t_n)\cos(m\pi/N_z), \\ Y_{m,n} &\approx A_y(t_n)\cos(m\pi/N_z), \end{aligned} \tag{23}$$

using least squares. The resulting time series for the buckling amplitude vector $(A_x(t), A_y(t))$ was then averaged through periods,

$$\langle A_{x,y}\rangle\left(\frac{T_{n+1}+T_n}{2}\right) = \frac{1}{T_{n+1}-T_n}\int_{T_n}^{T_n+1} A_{x,y}(t)\,dt,$$

with the time-integral implemented using the trapezoid rule. The periods were defined via u records at a selected point,

$$u(x_r, y_r, z_r, T_j) = u_*, \qquad \partial_t u(x_r, y_r, z_r, T_j) > 0,$$

which was typically chosen in the box corner, $(x_r, y_r, z_r) = (0,0,0)$. These period-averaged data were then used to define the amplitude $A = |\langle A_x\rangle + i\langle A_y\rangle|$ and phase $\Phi = \arg(\langle A_y\rangle / \langle A_x\rangle)$ of buckling. The buckling was considered established when the graph of $A(t)$ showed saturation, subject to residual numerical noise. The value of $A(t)$ average over a sufficiently long "established interval" of time was then used for graphs in figures 2(a) (top) and 3(a). The buckling phase was made "continuous", so the difference between consecutive readings of Φ does not exceed π, by transformation $\Phi(t) \mapsto \Phi(t) + 2\pi N_t$ with appropriately chosen $N_t \in \mathbb{Z}$. The resulting normalized dependence was approximated in the same established interval using least squares by a linear function of t, the slope of which gave the estimate of precession frequency Ω, used for fig. 2(a) (bottom).

For fig. 3(c), the buckling was so strong that the filament shape was not approximated well by Eqs. (23). There we took instead $A_x(t_n) = \frac{1}{2}(X_{N_z,n} - X_{0,n})$, $A_y(t_n) = \frac{1}{2}(Y_{N_z,n} - Y_{0,n})$ as the raw data.

B.3 Numerical evaluation of the rigidity coefficients

Computations of spiral wave solutions $\mathbf{U}$, their angular velocity ω_0, and their translational eigenmodes $|\mathbf{V}_+\rangle$ and $\langle\mathbf{W}^+|$ were performed by `dxspiral` suite [8] based on the method described in [9], which depends on three discretization parameters: the disk radius $\rho_{\max}$, radial resolution N_ρ and angular resolution N_θ. For the eigenvalue problems, we used straight shift-invert Arnoldi iterations without Cayley transform, and a Krylov dimensionality of 10. The list of computed quantities used in previous publications [9, 10] had to be extended to compute $e_1 + ie_2$, which involved the quasi-inversion process $|\mathbf{a}\rangle \mapsto |\mathbf{b}\rangle$, where

$$|\mathbf{b}\rangle = \hat{\mathbf{L}}'\hat{\pi}\,|\mathbf{a}\rangle$$

with $\hat{\mathbf{L}}'$ being the inverse $(\hat{\mathbf{L}} - i\omega_0)^{-1}$ in the subspace orthogonal to $\langle\mathbf{W}_+|$. Recall that $\hat{\pi}$ is the projection operator to that subspace, given by Eq. (19). Although the exact $\hat{\mathbf{L}}'$ is not defined in the whole space, its numerical implementation is defined, albeit extremely ill-posed. (For, the more accurate is the solution of the eigenvalue problems for $|\mathbf{V}_+\rangle$ and $\langle\mathbf{W}^+|$, the higher is the condition number of $\hat{\mathbf{L}}'$). Therefore, this computation presented some challenge.

To achieve satisfactory results, we applied the projection operator before and after the inverse, each several times,

$$|\mathbf{b}\rangle = \hat{\pi}^k\hat{\mathbf{L}}'\hat{\pi}^m\,|\mathbf{a}\rangle \tag{24}$$

where k and m were integers taken as large as to ensure that further applications of $\hat{\pi}$ did not change the results any more at a given floating point precision (we used 8-byte arithmetics). Obviously, the exact $\hat{\pi}$ and $\hat{\mathbf{L}}'$ commute, so mutliple applications of $\hat{\pi}$ would not change the result "in the ideal world", and in the real computations they minimized the impact of the round-off errors and the magnifying effect of the ill-posed $\hat{\mathbf{L}}'$.

Apart from straight application of the inverse $\hat{\mathbf{L}}'$ through LU decomposition, we also tried iterative application of the same, a version of GMRES method and Tikhonov regularization.

The quality of the quasi-inverse was assessed by normalized residual

$$\left|\left||\mathbf{a}\rangle - \hat{\mathbf{L}}\,|\mathbf{b}\rangle\right|\right| / \left|\left|\,|\mathbf{a}\rangle\right|\right|,$$

where the norm is in l_2. We found that with multiple application of $\hat{\pi}$, the simplest method gives a satisfactory quality (normalized residual of the order of 10^{-2} or less) which is not easily improved with the other, more time-consuming methods.

B.4 Continuation of the eigenvalue problem

Our method is similar to that used in [4], up to the choice of the eigenvalue solver. Solving the eigenvalue problem

$$\hat{\mathbf{L}}_{k_z}\,|\mathbf{V}(k_z)\rangle = \lambda(k_z)\,|\mathbf{V}(k_z)\rangle\,,$$

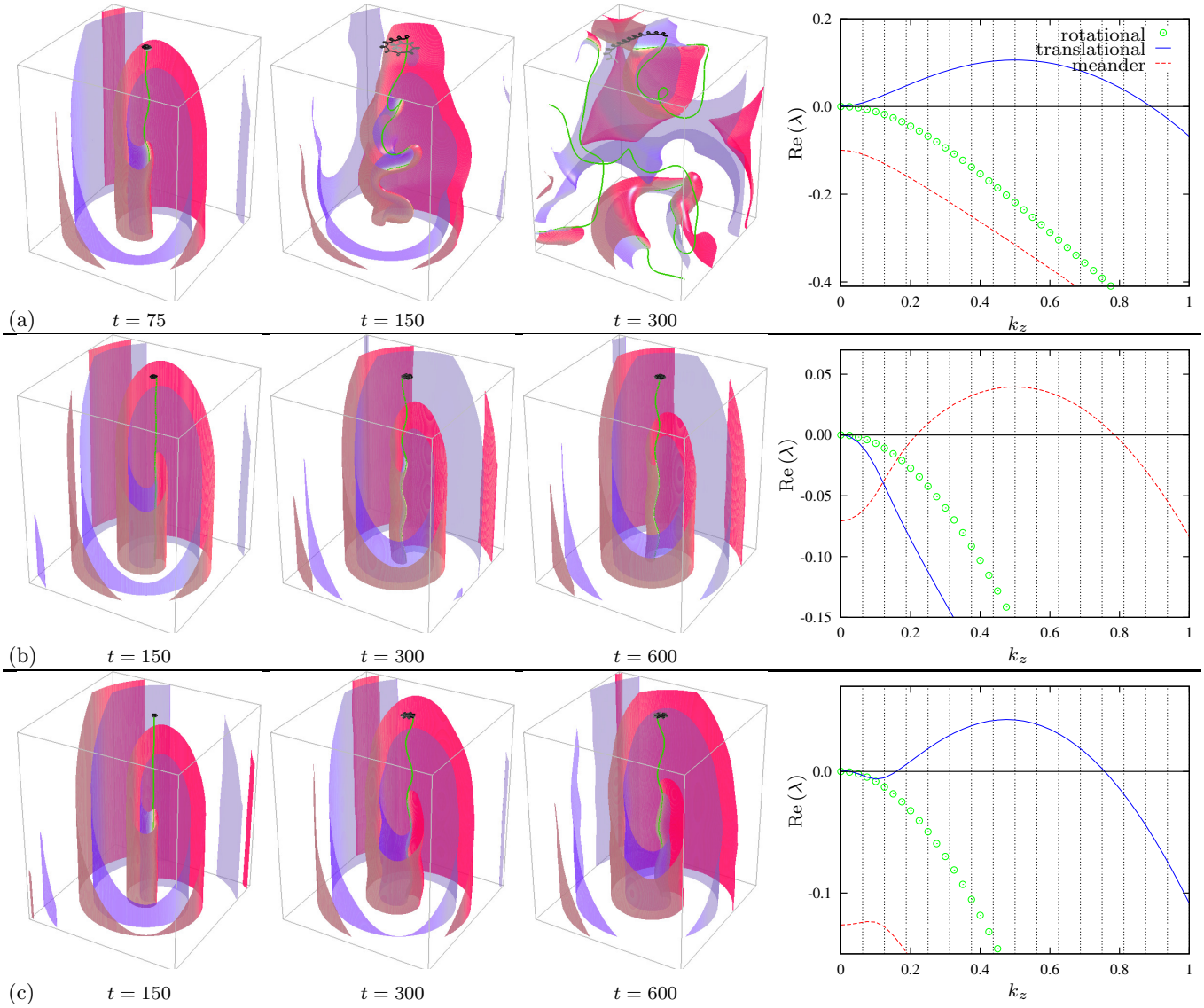

FIG. 5. Autowave turbulence vs wrinkled scrolls. (a), (b) correspond to fig. 4; (c) $a = 1.1$, $b = 0.17$, $c = 0.02$, $D_v = 0$. Box size $40 \times 40 \times 50$. The x-grid on the spectra represents the allowed wavenumbers nk_0, $n \in \mathbb{Z}$, $k_0 = \pi/L_z$, corresponding to the given box height $L_z = 50$.

by continuation in parameter k_z, starting from a known initial value $\lambda(0)$, was done at the same discretization as the unperturbed spiral wave solution $\mathbf{U}$ and the eigenmodes $|\mathbf{V}_+\rangle$ and $\langle\mathbf{W}^+|$ of the asymptotic theory. We used the following discretization parameters in calculating the eigenvalue branches: $\rho_{\max} = 25$, $N_\theta = 1000$, $N_\rho = 64$. The problem is fully resolved at these parameters, in the sense that further increase of either of them does not visibly change the graphs.

The rotational branch $\lambda_0(k_z)$ was obtained by continuation of the eigenvalue $\lambda_0(0) = 0$. The translational branch $\lambda_+(k_z)$ was continued from $\lambda_+(0) = i\omega_0$ where ω_0 was the angular velocity of the unperturbed spiral as found by `dxspiral`. Finding the starting point for the for the meandering branch $\lambda_m(k_z)$ was more complicated. We have used `EZRide` [11] to obtain a steady spiral wave solution starting from cross-field initial conditions. The "quotient data", representing relative velocity and angular velocity of the tip, were approaching their equilibria in an oscillatory manner. After manually eliminating an initial transient period, these data were approximated by a dependency of the form $\mathrm{Re}\left(Ae^{\lambda t}\right)$, $A, \lambda \in \mathbb{C}$, using Gnuplot implementation of the Marquard-Levenberg algorithm. Thus found λ was used as an initial guess for the `dxspiral` calculations at $k_z = 0$ and then for continuation in k_z to obtain the meandering branch.

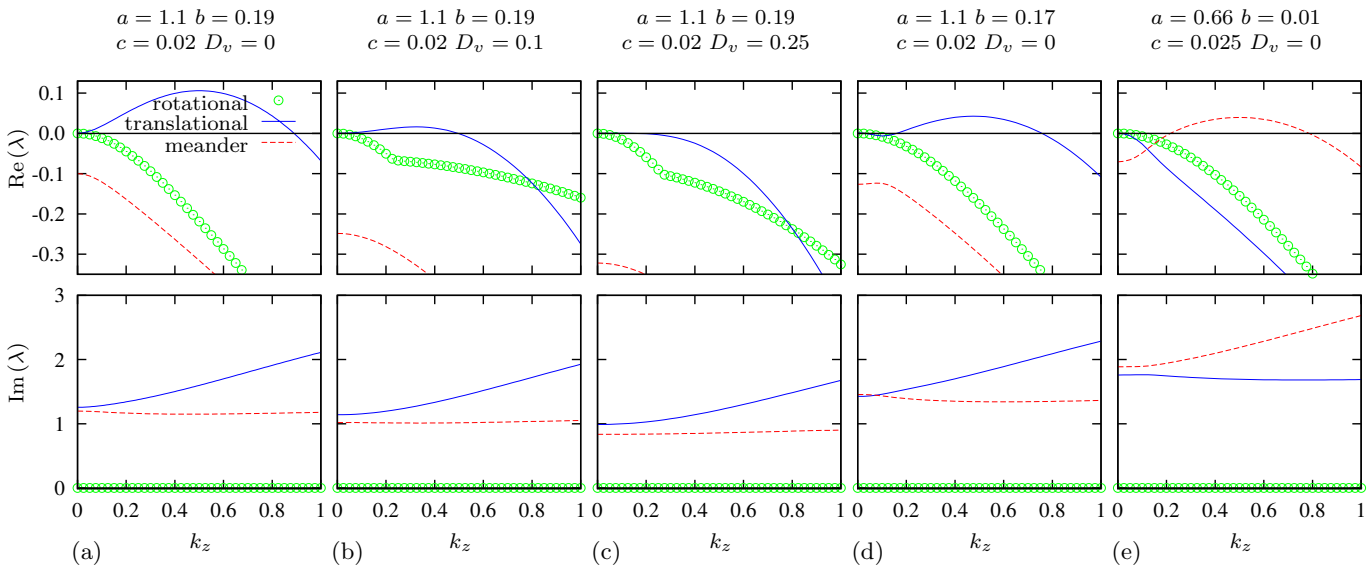

FIG. 6. Linearization spectra for all parameter sets used in the paper: (a) fig. 3(a,b), fig. 4(a),fig. 5(a); (b) fig. 1, fig. 2; (c) fig. 3(c,d); (d) fig. 5(c); (e) fig. 4(b), fig. 5(b).

C. Supplementary results

Fig. 5 expands on the comparison of the negative tension case leading to buckled scroll or scroll wave turbulence on one side, and the "3D meandering" instability leading to "wrinkled" scrolls on the other side. Here we have added an intermediate case (lower row), which shows an instability of a translational, rather than meandering, branch, however the instability is in an interval of k_z separated from 0. The resulting phenomenology is the same as with 3D meandering: a seemingly stable wrinkled scroll is observed. Hence it appears that for the stability of wrinkled scrolls it is essential that the range of unstable wavenumbers is separated from 0, rather than exactly which branch shows the instability. A rigorous nonlinear analysis for the two cases (b) and (c) would have to take into account that there are several unstable wavenumbers in each case.

Fig. 6 illustrates the linearization spectra for all the parameter sets considered in the paper, shown in the same ranges for comparison. It is evident that spectra (a)–(d) show an instability of the translational mode, and spectrum (e) shows an instability of the meandering mode, and this is not complicated by any "hybridization" described in [4]. The only evident hybridization is of the rotational mode, appearing as fracture points of the corresponding $\mathrm{Re}\,(\lambda)$ curves on panels (b) and (c). Note that for rotational branch $\mathrm{Im}\,(\lambda) \equiv 0$.

[1] D. Barkley and M. Dowle, "EZ-SCROLL: A code for simulating scroll waves," `http://www.warwick.ac.uk/~masax/Software/ez_software.html` (2007).

[2] P. L. T. Brian, A. I. Ch. E. Journal **7**, 367 (1961).

[3] B. Carnahan, H. A. Luther, and J. O. Wilkes, *Applied numerical methods* (John Wiley & Sons, Inc., New York, 1969).

[4] H. Henry and V. Hakim, Phys. Rev. E **65**, 046235 (2002).

[5] J. Keener, Physica D **31**, 269 (1988).

[6] V. N. Biktashev, A. V. Holden, and H. Zhang, Phil. Trans. Roy. Soc. Lond. ser. A **347**, 611 (1994).

[7] H. Verschelde, H. Dierckx, and O. Bernus, Phys. Rev. Lett. **99**, 168104 (2007).

[8] D. Barkley, V. N. Biktashev, I. V. Biktasheva, G. V. Bordyugov, and A. J. Foulkes, "DXSpiral: a code for studying spiral waves on a disk," `http://www.csc.liv.ac.uk/~ivb/software/DXSpiral.html`.

[9] I. V. Biktasheva, D. Barkley, V. N. Biktashev, G. V. Bordyugov, and A. J. Foulkes, Phys. Rev. E **79**, 056702 (2009).

[10] I. V. Biktasheva, D. Barkley, V. N. Biktashev, and A. J. Foulkes, Phys. Rev. E **81**, 066202 (2010).

[11] A. J. Foulkes and V. N. Biktashev, Phys. Rev. E **81**, 046702 (2010).